Supporting Information

Improved Photovoltaic Performance and Stability of Perovskite Solar Cells by Adoption of an n-Type Zwitterionic Cathode Interlayer

Young Wook Noh, †[a] Jung Min Ha, †[b] Jung Geon Son, [c] Jongmin Han, [a] Heunjeong Lee, [d] Dae Woo Kim, [a] Min Hun Hee, [b] Woo Gyeong Shin, [a] Shinuk Cho, [d] Jin Young Kim, [c] Myoung Hoon Song *[a] and Han Young Woo *[b]

[a] Y. W. Noh, J. Han, D. W. Kim, W. G. Shin, Prof. M. H. Song
School of Materials Science and Engineering, Ulsan National Institute of Science and Technology (UNIST), UNIST-gil 50, Ulsan, 44919, Republic of Korea.
*E-mail: mhsong@unist.ac.kr

[b] J. M. Ha, M. H. Jee, Prof. H. Y. Woo
Department of Chemistry, Korea University, Seoul 02841, Republic of Korea.
*E-mail: hywoo@korea.ac.kr

[c] J. G. Son, Prof. J. Y. Kim
School of Energy and Chemical Engineering, Ulsan National Institute of Science and Technology (UNIST), UNIST-gil 50, Ulsan, 44919, Republic of Korea.

[d] H. Lee, Prof. S. Cho
Department of Physics and EHSRC, University of Ulsan, Ulsan 44610, Republic of Korea.

Keywords: perovskite solar cells, zwitterion, cathode interlayer, ion capture, photovoltaic cells

Experimental Section

Materials

All chemicals used for the synthesis of the NDI molecules were purchased from Sigma-Aldrich and TCI Chemicals and used as received without further purification. [2-(3,6-Dimethoxy-9*H*-carbazol-9-yl)ethyl]phosphonic acid (MeO-2PACz, TCI), formamidinium iodide (FAI, Greatcell Solar), lead iodide (PbI_2, TCI), cesium iodide (CsI, ultra dry, 99.999% (metal basis), Alfa Aesar), fullerene (C_{60}, 99.99%, OSM), and silver (Ag, 1-4 mm shot, 99.9999%, iTASCO) were purchased and used without any further purification.

Synthesis

NDI-ZI and NDI-N were synthesized following the reported procedure.[1, 2]

NDI-N: ^{1}H NMR (500 MHz, $CDCl_3$): δ (ppm) 8.79 (s, 4H), 4.20 (t, 4H), 1.82 (m, 4H), 1.06 (t, 6H); ^{13}C NMR (125 MHz, $CDCl_3$): δ (ppm) 162.9 (C=O), 131.0 (Ar C), 126.7 (Ar C), 126.6 (Ar C), 42.4 (CH_2), 21.4 (CH_2), 11.5 (CH_3).

NDI-ZI: ^{1}H NMR (500 MHz, D_2O): δ (ppm) 8.63 (s, 4H), 4.22 (t, 4H), 3.47 (t, 4H), 3.33 (t, 4H), 3.07 (s, 12H), 2.83 (t, 4H), 2.22 (m, 4H), 1.87 (m, 4H), 1.72 (m, 4H); ^{13}C NMR (125 MHz, D_2O): δ (ppm) 164.0 (C=O), 131.1 (Ar C), 126.0 (Ar C), 125.9 (Ar C), 63.4 (CH_2-N), 61.5 (CH_2-N), 50.7 (CH_2-S), 49.9 (CH_3-N), 43.0 (CH_2), 37.7 (CH_2), 21.1 (CH_2), 20.9 (CH_2).

Instruments and Characterization

The ^{1}H and ^{13}C NMR spectra were measured using a Bruker Advance III HD system operating at 500 and 125 MHz, respectively. The UV-vis absorption spectra were measured using a Jasco V-730 UV-vis spectrometer. The absorption spectrum of tetramethylammonium iodide (TMAI) + I_2 was obtained from a 2:1 (w/w) mixture of TMAI and solid I_2 dissolved in water at a total concentration of 2%. The absorption spectrum of gaseous I_2 was obtained by heating the solid I_2 at 50 ^{o}C in an N_2-purged PMMA cuvette. To measure the absorption spectra of the NDI films

with I_2 gas, the NDI derivatives were dissolved in trifluoroethanol (2 mg/mL) and spin-coated onto a glass substrate at 2000 rpm. The NDI-ZI and NDI-N films were heated together for 30 min in a Petri dish with a 1:1 mixture of solid I_2 and silica gel (2 g) under ambient conditions. The distribution of silver in the perovskite/C_{60}/NDI-ZI/silver sandwich cell was analyzed using ToF-SIMS (ION-TOF, Germany) with Bi^{3+} (30 keV) as the primary ion source. The area of analysis was 100 μm × 100 μm. Sputter etching was performed using an Ar-gas cluster ion beam with an accelerating voltage of 2.5 keV. The *J-V* characteristics of the PeSCs were measured under AM 1.5 G (100 mW cm^{-2}) with a scan rate of 300 mV s^{-1} and scan step of 10 mV. A PEC-L01 solar simulator was used for illumination, and the intensity was calibrated using a Newport 91150-KG5 Si reference cell. Scanning electron microscopy images and energy-dispersive X-ray spectroscopy data were obtained using an SU8220 Cold FESEM operated at 10 kV. UPS (AXIS Nova, Kratos Analytical) measurements were performed using a He (21.2 eV) ultraviolet source. X-ray photoelectron spectroscopy was performed using a K-alpha system operating from 200 to 3 keV. TPC and TPV data were measured using a T4000 instrument (McScience). The external quantum efficiency spectra were measured using a QEX7 quantum efficiency measurement system. An antireflection film was fabricated using polydimethylsiloxane cast on a fluorinated random pyramid-textured Si wafer as a mold.[3]

Device Fabrication

ITO-coated glass substrates were first washed sequentially with deionized water, acetone, and isopropyl alcohol under sonication for 10 minutes. Subsequently, the cleaned substrates underwent treatment with UV-O_3 for 30 minutes and were then transferred to a N_2 glove box. MeO-2PACz (1 mg mL^{-1} in ethanol) was spin-coated at 5000 rpm for 30 seconds, followed by annealing at 100 °C for 10 minutes. After cooling, the films were rinsed by spin-casting ethanol solvent at 5000 rpm for 25 seconds. For the $FA_{0.85}Cs_{0.15}PbI_3$ precursor, 1.445 mmol of FAI, 0.255 mmol of CsI, and 1.7 mmol of PbI_2 were dissolved in 700 μL DMF and 300 μL DMSO.

The perovskite precursor solution was spin-coated at 500 rpm for 7 seconds and then at 3000 rpm for 25 seconds. After 21 seconds, ethyl acetate (0.45 mL) was added on top of the perovskite layer during spin-coating. Thermal annealing at 100 °C for 1 hr followed. A 30-nm-thick C_{60} layer was then deposited under high vacuum (< 5×10^{-6} torr) at an evaporation rate of 0.3 Å/s. The NDI-ZI layer was spin-coated onto the C_{60} layer at 5000 rpm for 30 seconds, followed by annealing at 100 °C for 10 minutes. Finally, a 100-nm-thick silver electrode was thermally deposited under high vacuum. The device area (13.5 mm^2) was defined by the patterned metal mask used for the thermal deposition of silver.

a

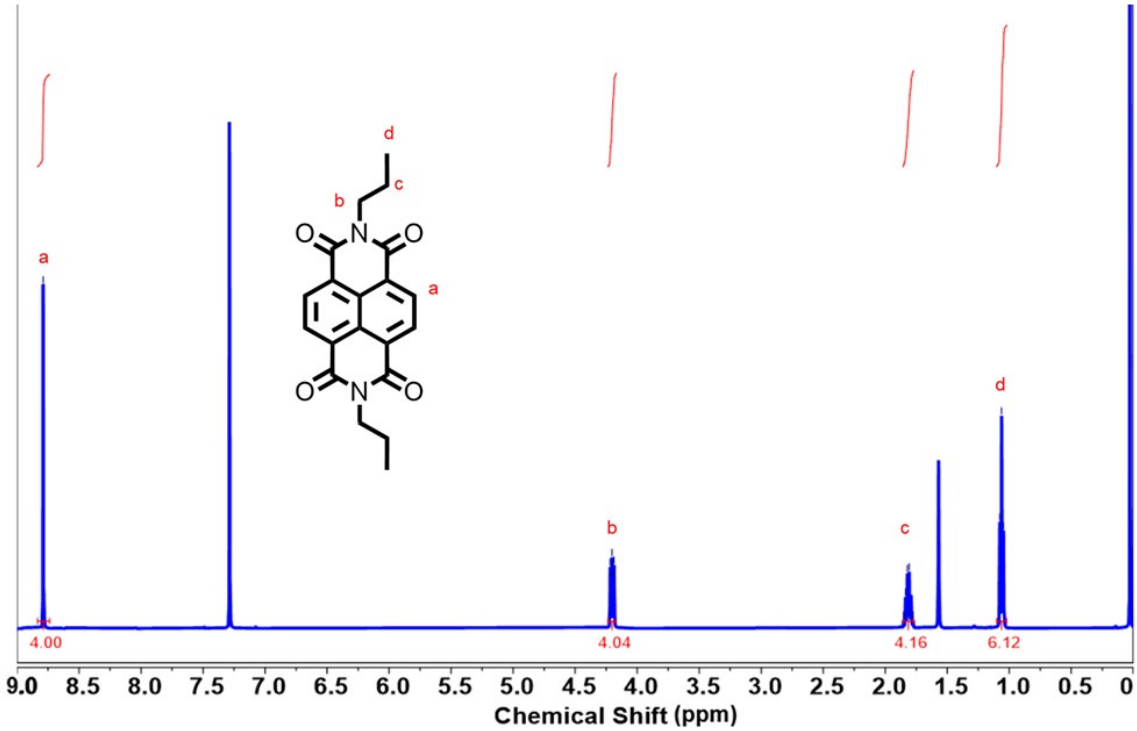
a
b
c
d
4.00
4.04
4.16
6.12
9.0 8.5 8.0 7.5 7.0 6.5 6.0 5.5 5.0 4.5 4.0 3.5 3.0 2.5 2.0 1.5 1.0 0.5 0
Chemical Shift (ppm)

b

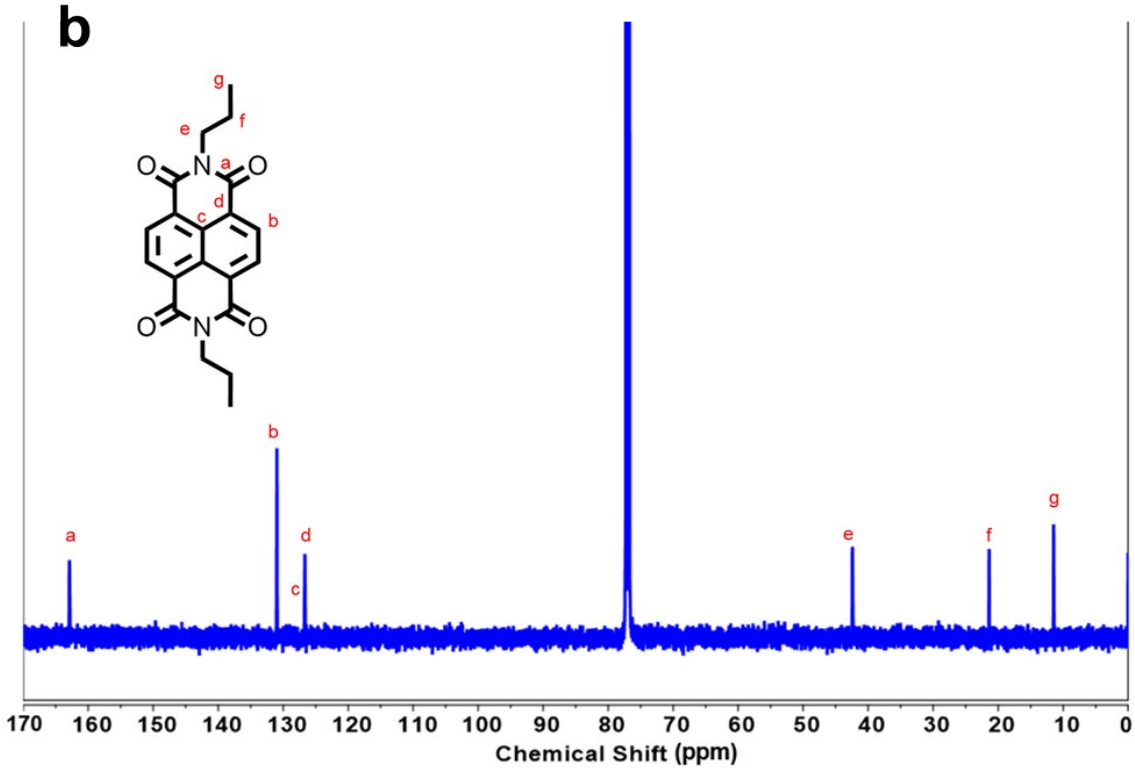
a
b
c
d
e
f
g
170 160 150 140 130 120 110 100 90 80 70 60 50 40 30 20 10 0
Chemical Shift (ppm)

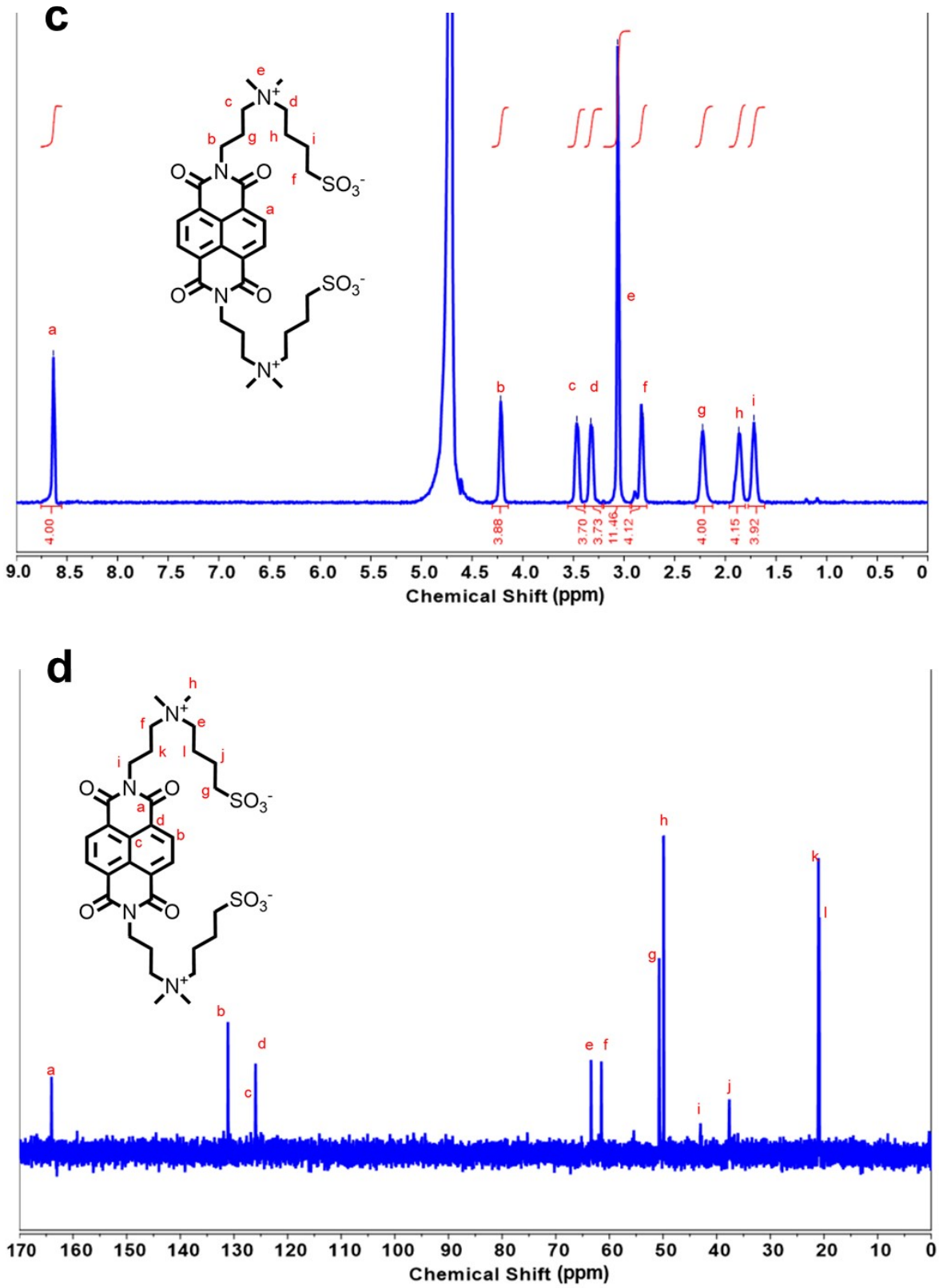

Fig. S1 (a) ^{1}H-NMR and (b) ^{13}C-NMR spectra of NDI-N in $CDCl_3$. (c) ^{1}H-NMR and (d) ^{13}C-NMR spectra of NDI-ZI in D_2O.

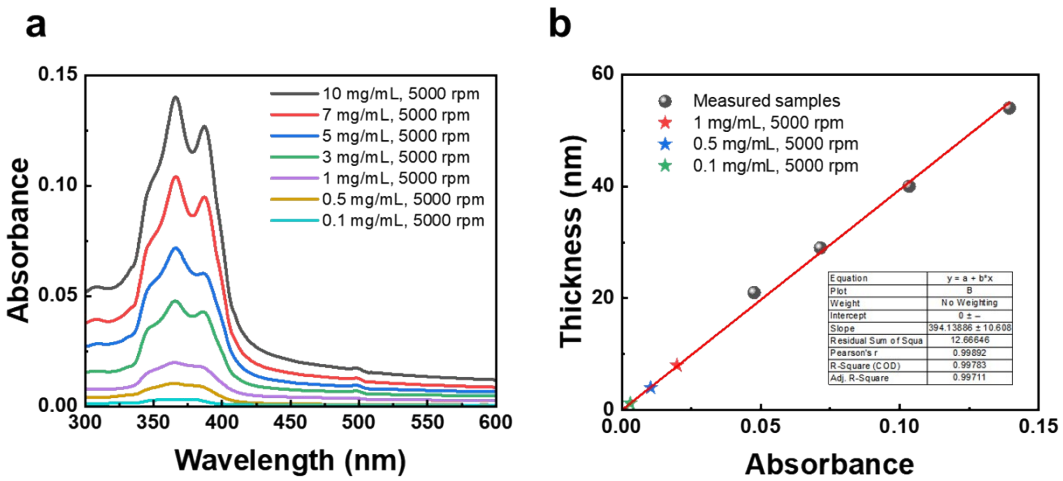

Fig. S2 (a) UV-vis absorbance spectra of NDI-ZI thin films with different concentrations. (b) Linear fitting of absorbance versus thickness of NDI-ZI films.

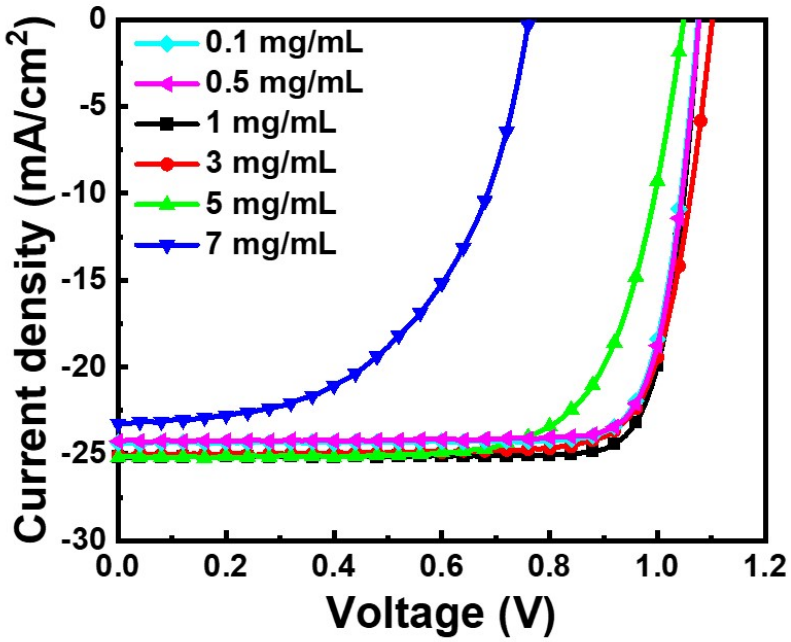

Fig. S3 *J-V* curves of PeSCs by varying the thickness of NDI-ZI interlayer.

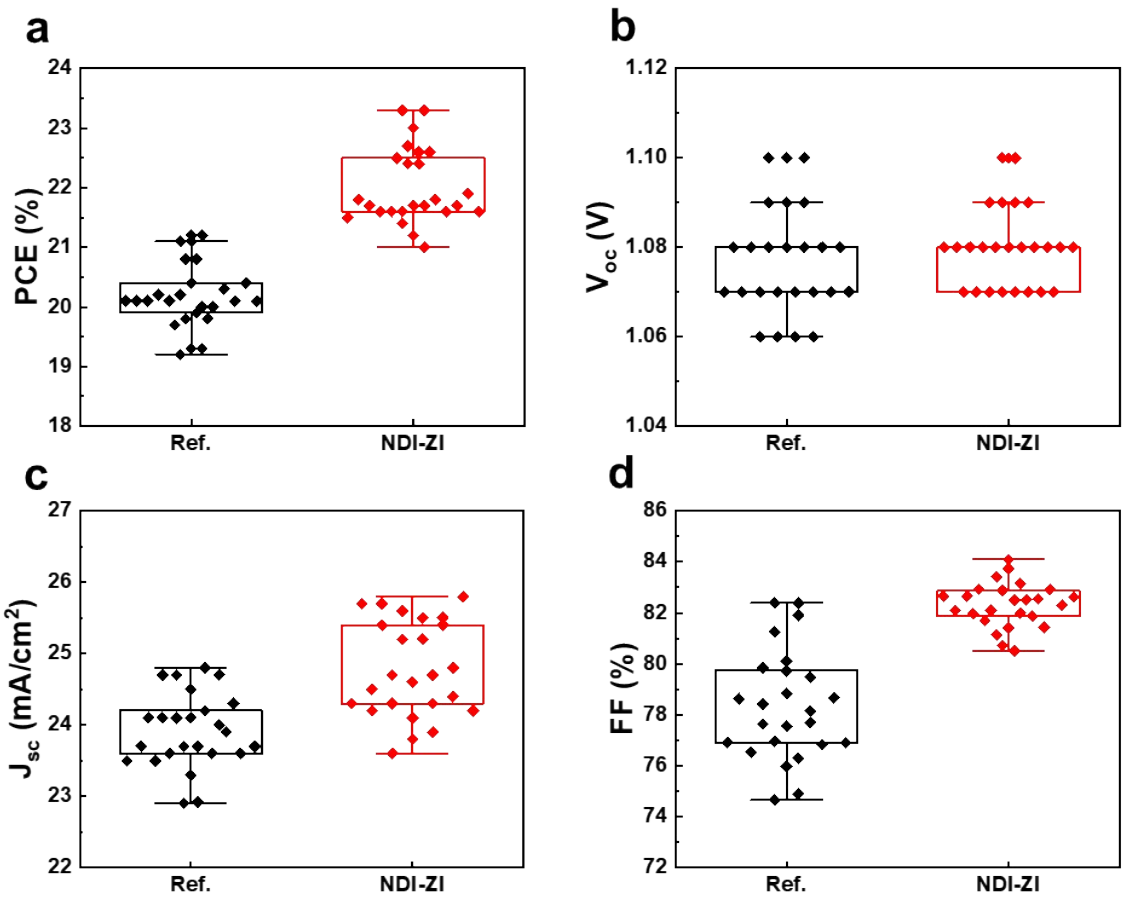

Fig. S4 Statistical photovoltaic data of (a) PCE, (b) V_{OC}, (c) J_{SC}, and (d) FF for PeSCs with and without NDI-ZI (based on 25 separated measurements).

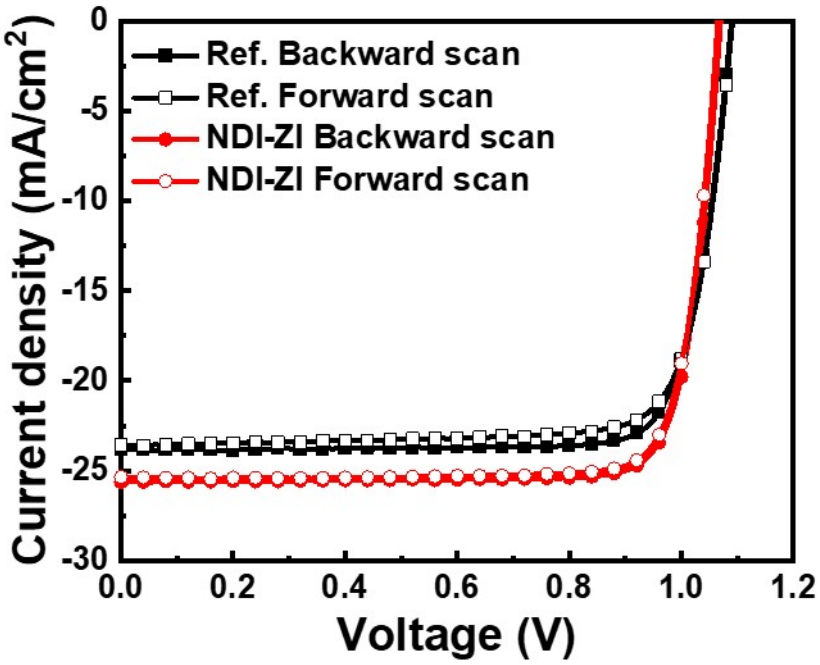

Fig. S5 *J-V* curves of PeSCs with and without NDI-ZI interlayer under both backward and forward scans.

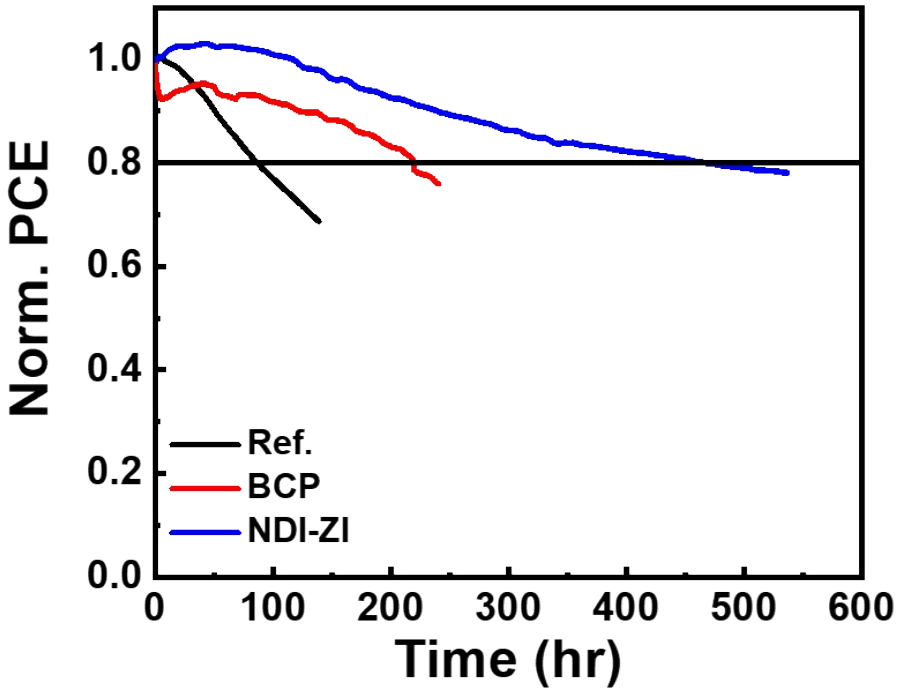

Fig. S6 Device stability at MPP condition (AM 1.5G illumination) without, with BCP, and with NDI-ZI cathode interlayer.

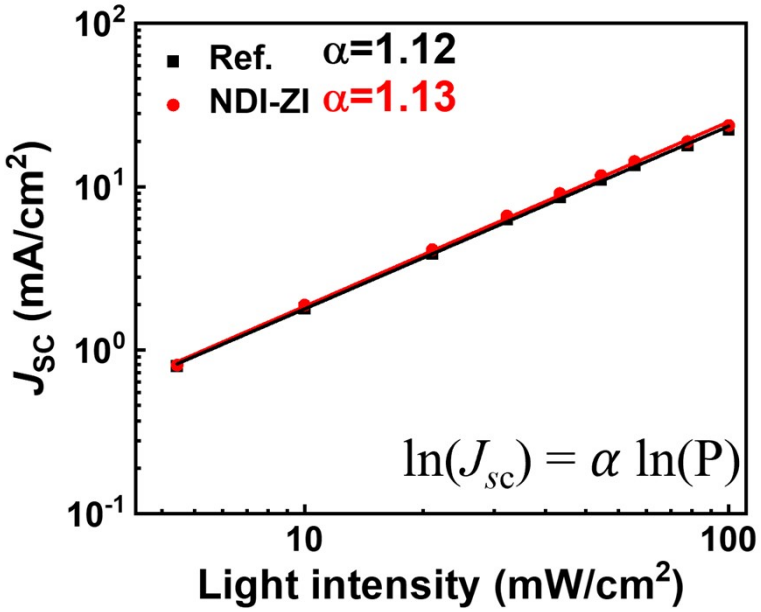

Fig. S7 Light intensity dependent J_{SC} characteristics with and without NDI-ZI.

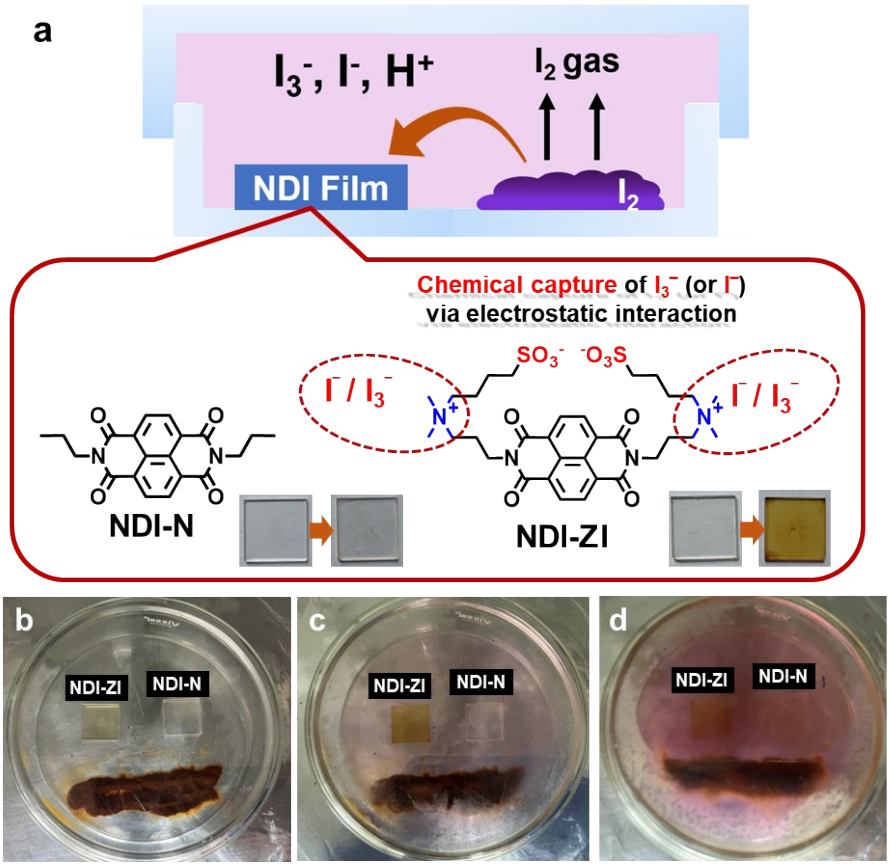

Fig. S8 (a) Schematic of I^- and I_3^- capture of NDI films under I_2 sublmation. Photographic images of NDI-N and NDI-ZI films exposed to I_2 sublimation at different temperatures; (b) room temperature, (c) 90 °C, (d) 120 °C.

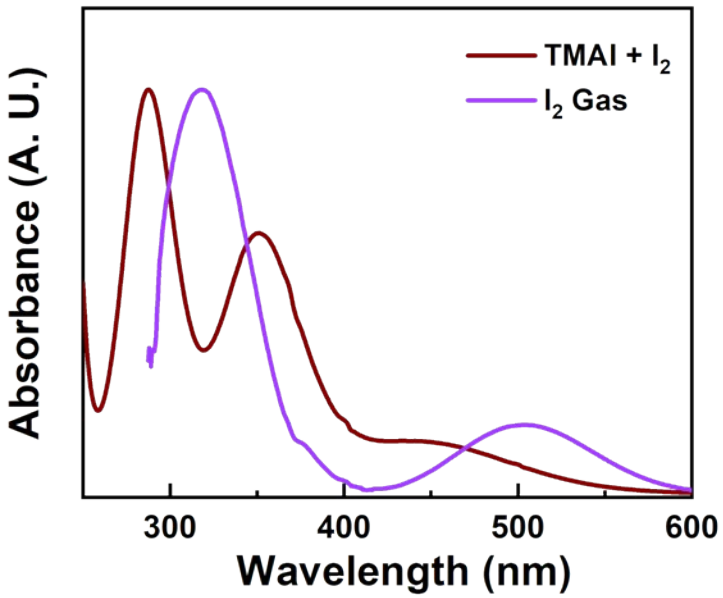

Fig. S9 UV-vis absorption spectra of a mixture (1:1 mol%) of tetramethyl ammonium iodide and I_2 in water, and iodine gas.

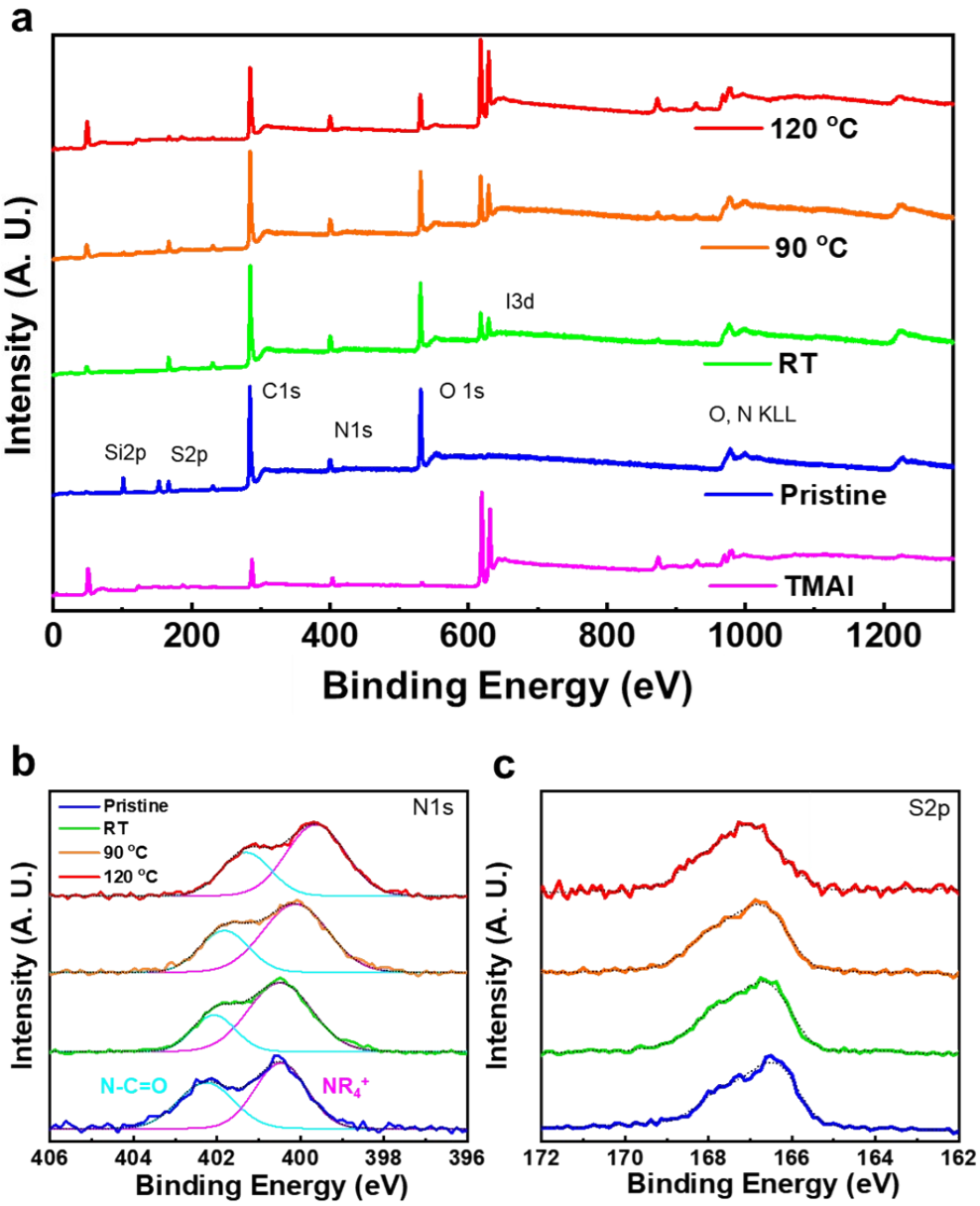

Fig. S10 XPS measurements. (a) survey mode spectra, and core level spectra of (b) N 1s and (c) S 2p core electrons obtained from NDI-ZI films exposed to iodine gas at different temperature.

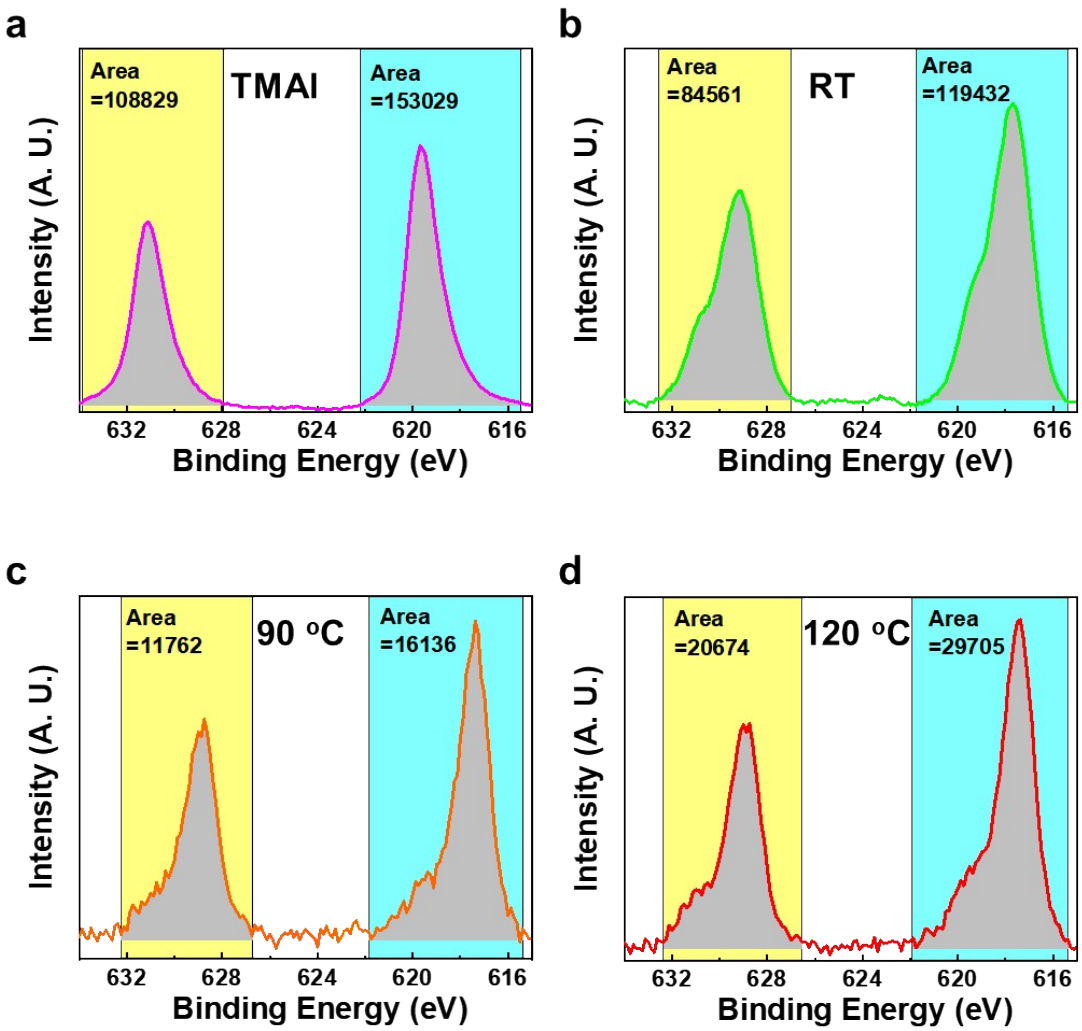

Fig. S11 XPS peak area ($3d_{5/2}$:$3d_{3/2}$) of (a) TMAI (as a reference) and NDI-ZI films exposed to iodine gas at (b) RT, (c) 90 °C, and (d) 120 °C.

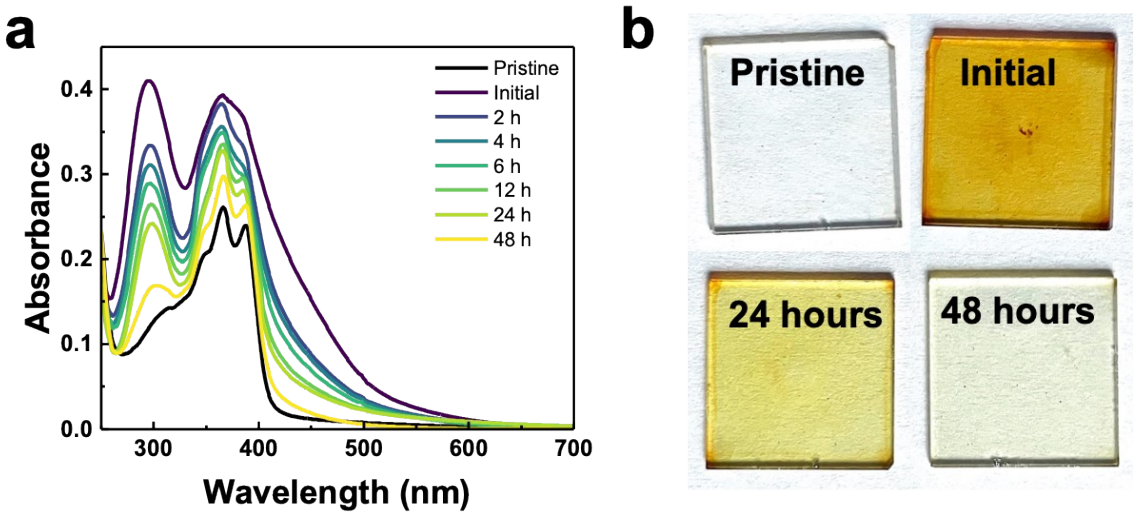

Fig. S12 (a) UV-vis spectral changes and (b) photographic images of NDI-ZI films (exposed to I_2 sublimation) stored in an ambient environment.

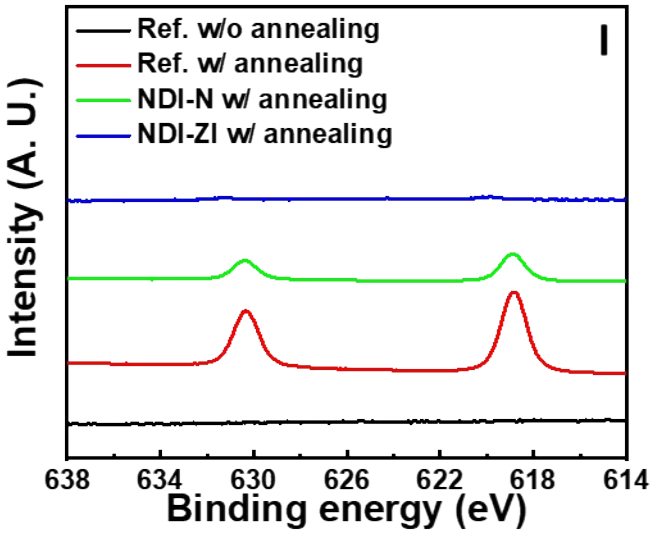

Fig. S13 I 3d XPS signals of top surface of Ag electrode with a thermal treatment at 120 °C for 24 hrs.

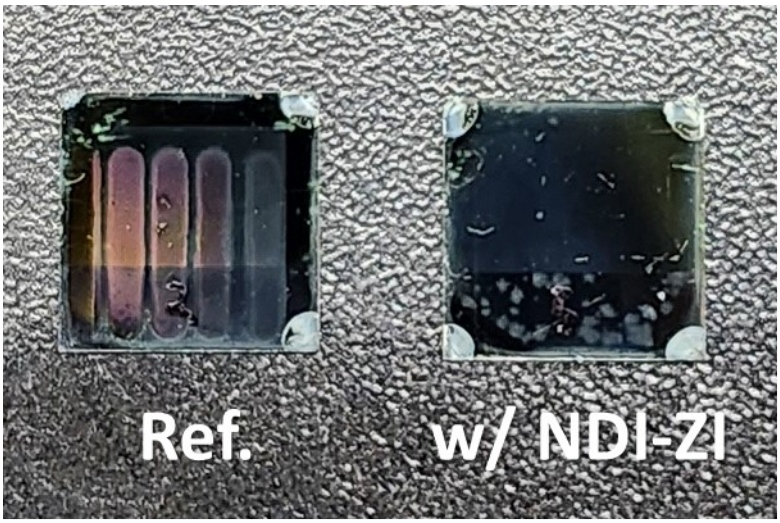

Fig. S14 Photographic images of PeSCs with and without NDI-ZI after thermal treatments at 120 ^{o}C for 24 hrs.

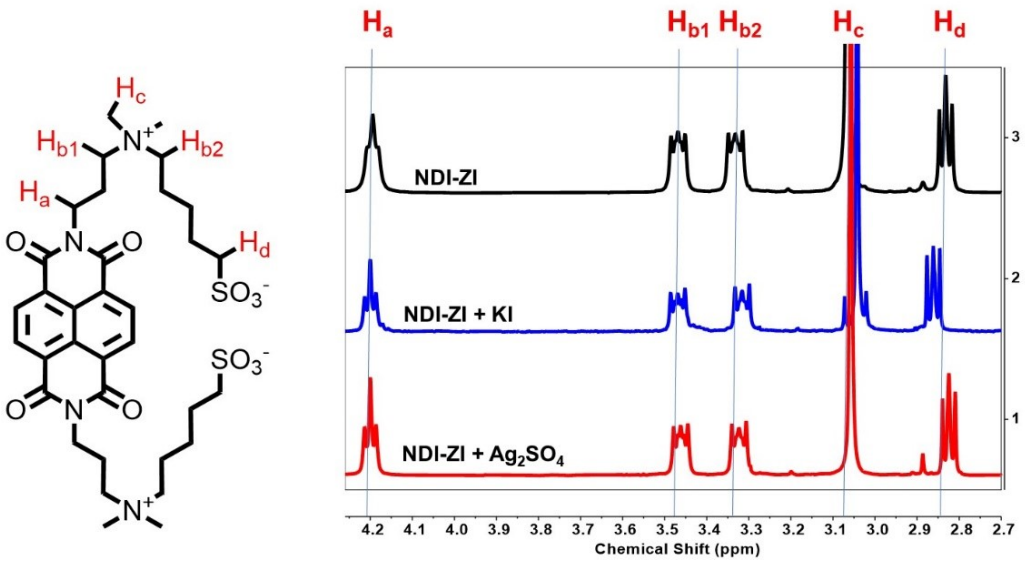

Fig. S15 ^{1}H NMR spectra of NDI-ZI without and with KI or Ag_2SO_4 in D_2O. ^{1}H NMR analysis was also conducted with NDI-ZI dissolved in deuterium oxide (D_2O) in the presence of 10 equivalents of KI or Ag_2SO_4. In the case of proton H_a at 4.22 ppm, which is close to N of imide with no ionic interaction with KI or Ag_2SO_4, no shift of peak position was observed. Meanwhile, the proton peaks near quaternary N^+ (H_b, H_c) and $-SO_3^-$ (H_d) of NDI-ZI are clearly shifted by adding external ion source, due to the change in the dynamic ionic coulombic interaction. Upon addition of excess KI, the ionic NR_4^+ and RSO_3^- groups have coulombic interaction with I^- and K^+, respectively. According to the NMR spectra (shown in Figure R2), upshift of H_{b2} and H_c peaks was observed from 3.33 and 3.07 ppm to 3.31 and 3.04 ppm, respectively. The upshift originated from that the ionic interaction of $NR_4^+ - RSO_3^-$ is changed into $NR_4^+ - I^-$. Similarly, the downshift of H_d (from 2.83 to 2.86 ppm) can be understood in terms of a new ionic interaction of $RSO_3^- - K^+$. When excess Ag_2SO_4 was mixed with NDI-ZI, the H_d peak showed a clear upshift (from 2.83 to 2.81 ppm) due to formation of coulombic interaction between RSO_3^- and Ag^+. The NMR data strongly support that zwitterionic NDI-ZI have ionic coulombic interactions with both positive and negative ions.

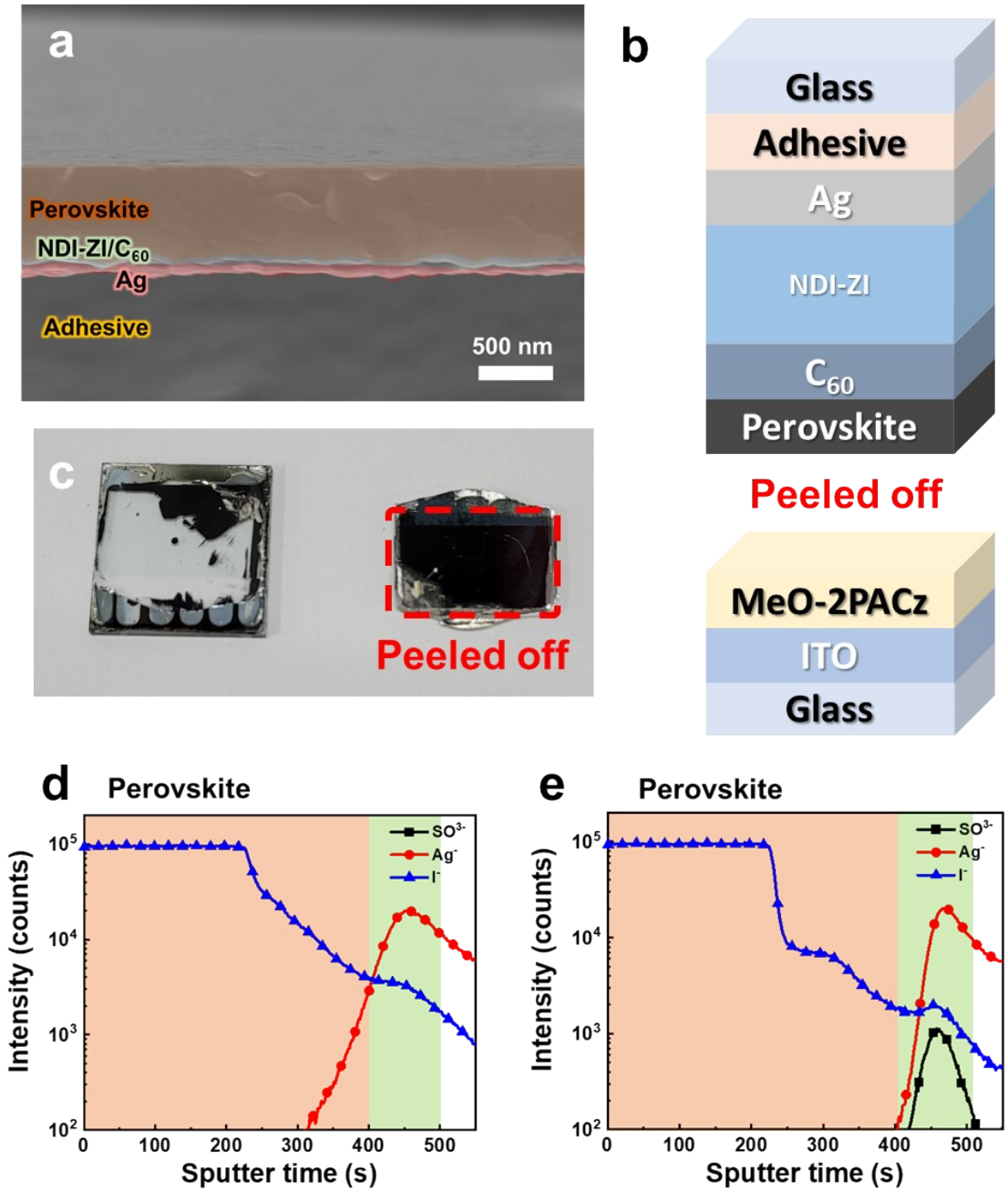

Fig. S16 (a) Cross-sectional SEM, (b) device structure, and (c) photographic images of peeled off perovskite films from device. ToF-SIMS depth profiles of (d) without and (e) with NDI-ZI layer after light soaking test for 500 hrs under continuous 1-sun illumination at room temperature and RH 25%.

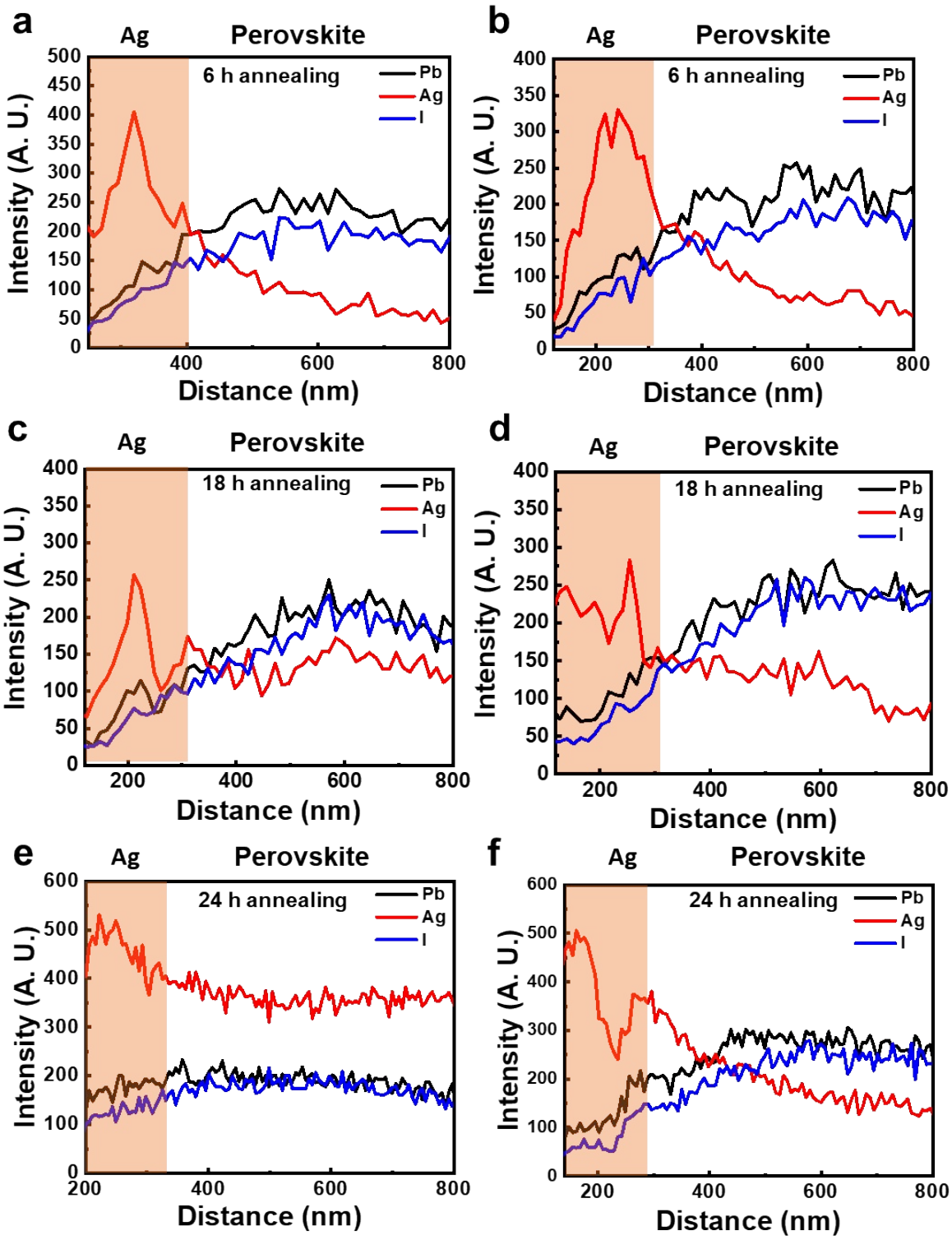

Fig. S17 EDS linecut depth profiles of PeSCs without (a, c, and e) and with NDI-ZI (b, d, and f) after thermal treatments at 90 °C by varying the annealing time. Reference devices annealed for (a) 6 hrs, (c) 18 hrs, and (e) 24 hrs. Devices with NDI-ZI annealed for (b) 6 hrs, (d) 18 hrs, and (f) 24 hrs.

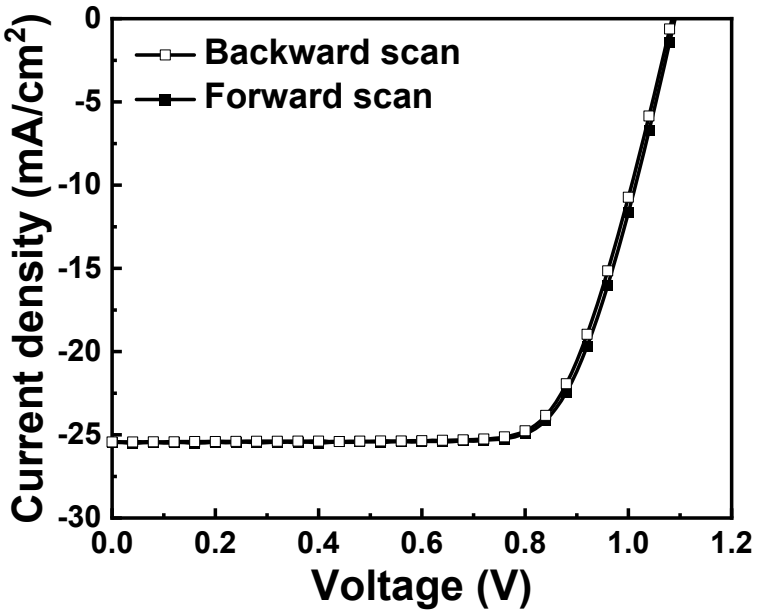

Fig. S18 *J-V* curves of 1 cm^2 area PeSCs with NDI-ZI with anti-reflection film under backward and forward scans.

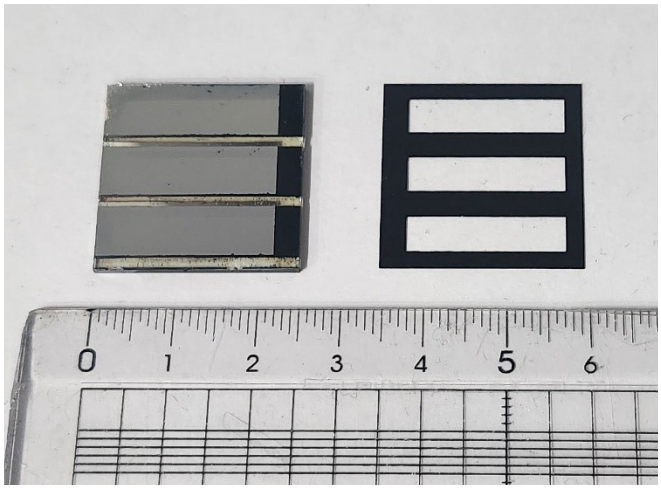

Fig. S19 Photographic images of mini module and aperture mask.

Table S1 Photovoltaic parameters of PeSCs by varying the thickness of NDI-ZI interlayer.

[NDI-ZI]	V_{OC} [V]	J_{SC} [mA cm^{-2}]	FF [%]	PCE [%]
0.1 mg/mL	1.08	24.40	82.16	21.60
0.5 mg/mL	1.08	24.30	82.48	21.60
1 mg/mL	1.08	25.20	82.84	22.50
3 mg/mL	1.10	25.10	78.18	21.80
5 mg/mL	1.05	25.20	71.29	18.90
7 mg/mL	0.77	23.30	53.00	9.50

Table S2 Photovoltaic parameters of PeSCs with and without NDI-ZI interlayer under backward and forward scans.

	Scan direction	V_{OC} [V]	J_{SC} [mA cm^{-2}]	FF [%]	PCE [%]	HI[a] [%]
Ref.	Backward	1.09	23.84	81.42	21.16	3.1
	Forward	1.09	23.60	79.60	20.50	
w/ NDI-ZI	Backward	1.07	25.60	83.15	22.80	1.3
	Forward	1.06	25.30	83.80	22.50	

[a]Hysteresis index.

Table S3 Photovoltaic parameters of large-area (1 cm^2) PeSCs with NDI-ZI interlayer under backward and forward scans.

Scan direction	V_{OC} [V]	J_{SC} [mA cm^{-2}]	*FF* [%]	PCE [%]	HI[a] [%]
Backward	1.10	25.50	72.32	20.30	0.98
Forward	1.08	25.40	72.98	20.10	

[a]Hysteresis index.

Table S4. Summarized performance and device stability of inverted PeSCs reported in the previous studies.

Structure	*PCE* [%]	*Stability* [h]	*Condition*	MPP tracking [h]	Ref.
ITO/MeO-2PACz/ $Cs_{0.05}(MA_{0.1}FA_{0.9})_{0.95}Pb(I_{0.9}Br_{0.1})_3$/MPA/2D perovskite/PCBM/BCP/Ag	24.85	800 (92%)	unencapsulated RH 60%	NA	4
ITO/MeO-2PACz/ $Cs_{0.05}(FA_{0.98}MA_{0.02})_{0.95}Pb(I_{0.98}Br_{0.02})_3$/PCBM/BCP/Ag	24.6	NA	NA	1000 (96%)	5
FTO/NiOx/Me-4PACz/DPPP/$FA_{0.95}Cs_{0.05}PbI_3$/PEAI/C_{60}/SnO_2/Ag	23.9	1500 (90%)	85 °C	3500 (100%<)	6
ITO/PTAA/ $(FA_{0.98}MA_{0.02})_{0.95}Cs_{0.05}Pb(I_{0.95}Br_{0.02})_3$/$FcTc_2$/$C_{60}$/BCP/Ag	24.5	1000 (95%)	85 °C/RH 85%	1500 (98%)	7
ITO/NiO_x/PTAA/Al_2O_3/$FA_{0.95}Cs_{0.05}PbI_3$/ PCBM/BCP/Ag	24.67	864 (98%)	85 °C	1008 (84%)	8
ITO/PTAA/Al_2O_3/$FA_{0.83}Cs_{0.17}Pb(I_{0.8}Br_{0.2})_3$/ LiBr/$C_{70}$/Zr(acac)4/Au	20.2	1410 (80%)	MPP/ 65 °C	NA	9
FTO/NiOx/4PACz/$(Cs_{0.05}MA_{0.05}FA_{0.90}PbI_3)_{0.95}(MAPbCl_3)_{0.05}$/ DMDP/$C_{60}$/BCP/Ag	25.9	1600 (95%)	85 °C	2000 (96%)	10
ITO/DMAcPA+CsFAMAPb(I_x	25.4	NA	NA	1000	11

$Br_y)_3$/PCBM/BCP/Ag				(96.6%)	
FTO/2PACz+3-MPA/$Cs_{0.05}MA_{0.1}FA_{0.85}PbI_3$ + MACl+GuaSCN/C_{60}/BCP/Ag	24.8	1000 (95%)	AM 1.5G/65 °C/RH 85%	NA	12
ITO/PTAA/perovskite/C_{60}/BCP/Ag	25.8%	300 (90%)	AM 1.5G/65 °C/RH 85%	2500 (92%)	13
ITO/2-PACZ/$FA_{0.85}MA_{0.1}Cs_{0.05}PbI_3$/$C_{60}$/BCP/Cu	25.6	400 (89%)	85 °C/RH 85%	1000 (94%)	14
FTO/NiO_x/Me-4PACz/$FAPbI_3$/PCBM/SnO_2/Cu	25.2	500 (85%)	85 °C	1000 (85%)	15
ITO/NiO_x/MeO-4PADBC/$Cs_{0.05}FA_{0.85}MA_{0.1}PbI_3$/$C_{60}$/BCP/Ag	25.6	1200 (74%)	85 °C	1200 (96%)	16
ITO/2PACz/$Cs_{0.05}FA_{0.8}MA_{0.15}PbI_3$/$C_{60}$/BCP/Ag	24.09	1600 (85%)	85 °C/RH 50%	NA	17
ITO/Al_2O_3/PTAA/NiOx/$Cs_{0.05}FA_{0.95}PbI_3$/PCBM/BCP/Ag	25.16	1200 (92%)	85 °C/RH 85%	1500 (98%)	18
ITO/Me-4PACz/$Cs_{0.05}FA_{0.8}MA_{0.15}Pb(I_{0.75}Br_{0.25})_3$+Me-4PACz/$C_{60}$/BCP/Ag	24.50	NA	NA	1200 (91%)	19
ITO/p-PY/$Cs_{0.02}FA_{0.98}PbI_3$+DBSO/2-CF_3-PEAI/PCBM/BCP/Ag	25.1	1000 (98%)	85 °C/RH 85%	1800 (97%)	20
ITO/NiO_x/Me-4PACz+PC/$Cs_{0.05}(FA_{0.98}MA_{0.02})_{0.95}Pb(I_{0.98}Br_{0.02})_3$/PEABr/PCBM+$C_{60}$/BCP/Ag	25.09	NA	NA	1000 (90%)	21
NiO_x/p-F-PEAI/$Cs_{0.05}FA_{0.85}MA_{0.1}Pb_3$/$C_{60}$/BCP/Cu	22.93	1000 (85%)	RH 50%	700 (80%)	22
ITO/MeO-2PACz/$FA_{0.85}Cs_{0.15}PbI_3$/C_{60}/NDI-ZI/Ag	23.30	1500 (80%)	85 °C	450 (80%)	This work

*Parentheses indicate the ratio of PCE to the initial PCE after stability test.
*The stability tests were listed with their methods and the ISOS-L-1 protocol was chosen as the MPP tracking standard (1-sun illumination, ambient temperature).

References

1. Q. Liao, Q. Kang, Y. Yang, Z. Zheng, J. Qin, B. Xu and J. Hou, *CCS Chem*. 2022, **4**, 938.
2. Y. Miyake, T. Nagata, H. Tanaka, M. Yamazaki, M. Ohta, R. Kokawa and T. Ogawa, *ACS Nano* 2012, **6**, 3876.
3. A. K. Harit, E. D. Jung, J. M. Ha, J. H. Park, A. Tripathi, Y. W. Noh, M. H. Song and H. Y. Woo, *Small* 2022, **18**, 2104933.
4. X. Zang, S. Xiong, S. Jiang, D. Li, H. Wu, H. Ren, A. Cao, B. Li, Z. Ma, J. Chen, L. Ding, J. Tang, Z. Sun, J. Chu and Q. Bao, *Adv. Mater*. 2023, 2309991.
5. G. Li, Z. Su, L. Canil, D. Hughes, M. H. Aldamasy, J. Dagar, S. Trofimov, L. Wang, W. Zuo, J. J. Jerónimo-Rendon, M. M. Byranvand, C. Wang, R. Zhu, Z. Zhang, F. Yang, G. Nasti, B. Naydenov, W. C. Tsoi, Z. Li, X. Gao, Z. Wang, Y. Jia, E. Unger, M. Saliba, M. Li and A. Abate, *Science* 2023, **379**, 399-403.
6. C. Li, X. Wang, F. Jiang, S. M. Park, Y. Li, L. Chen, Z. Wang, L. Zeng, H. Chen, Y. Liu, C. R. Grice, A. Abudulimu, J. Chung, Y. Xian, T. Zhu, H. Lai, B. Chen, R. J. Ellingson, F. Fu, D. S. Ginger, Z. Song, E. H. Sargent and Y. Yan, *Science* 2023, **379**, 690-694.
7. Z. Li, B. Li, X. Wu, S. A. Sheppard, S. Zhang, D. Gao, N. J. Long and Z. Zhu *Science* 2022, **376**, 416-420.
8. C. Zhang, H. Li, C. Gong, Q. Zhuang, J. Chen Z. Zang, *Energy Environ. Sci.* 2023, **16**, 3825-3836.
9. D. P. McMeekin, P. Holzhey, S. O. Furer, S. P. Harvey, L. T. Schelhas, J. M. Ball, S. Mahesh, S. Seo, N. Hawkins, J. Lu, M. B. Johnston, J. J. Berry, U. Bach and H. J. Snaith *Nat. Mater.* 2023, **22**, 73-83.

10. C. Liu, Y. Yang, H. Chen, J. Xu, A. Liu, A. S. R. Bati, H. Zhu, L. Grater, S. S. Hadke, C. Huang, V. K. Sangwan, T. Cai, D. Shin, L. X. Chen, M. C. Hersam, C. A. Mirkin, B. Chen, M. G. Kanatzidis and E. H. Sargent, *Science* 2023, **382**, 810-815.
11. Q. Tan, Z. Li, G. Luo, X. Zhang, B. Che, G. Chen, H. Gao, D. He, G. Ma, J. Wang, J. Xiu, H. Yi, T. Chen and Z. He, *Nature* 2023, **620**, 545–551.
12. S. M. Park, M. Wei, N. Lempesis, W. Yu, T. Hossain, L. Agosta, V. Carnevali, H. R. Atapattu, P. Serles, F. T. Eickemeyer, H. Shin, M. Vafaie, D. Choi, K. Darabi, E. D. Jung, Y. Yang, D. B. Kim, S. M. Zakeeruddin, B. Chen, A. Amassian, T. Filleter, M. G. Kanatzidis, K. R. Graham, L. Xiao, U. Rothlisberger, M. Grätzel and E. H. Sargent, *Nature* 2023, **624**, 289-294.
13. Z. Liang, Y. Zhang, H. Xu, W. Chen, B. Liu, J. Zhang, H. Zhang, Z. Wang, D. Kang, J. Zeng, X. Gao, Q. Wang, H. Hu, H. Zhou, X. Cai, X. Tian, P. Reiss, B. Xu, T. Kirchartz, Z. Xiao, S. Dai, N. Park, J. Ye and X. Pan, *Nature* 2023, **624**, 557-563.
14. P. Zhu, D. Wang, Y. Zhang, Z. Liang, J. Li, Z. Zeng, J. Zhang, Y. Xu, S. Wu, Z. Liu, X. Zhou, B. Hu, F. He, L. Zhang, X. Pan, X. Wang, N. G. Park and B. Xu, *Science* 2024, **383**, 524-531.
15. S. Yu, Z. Xiong, H. Zhou, Q. Zhang, Z. Wang, F. Ma, Z. Qu, Y. Zhao, X. Chu, X. Zhang and J. You, *Science* 2023, **382**, 1399-1404.
16. Z. Li, X. Sun, X. Zheng, B. Li, D. Gao, S. Zhang, X. Wu, S. Li, J. Gong, J. M. Luther, Z. Li and Z. Zhu, *Science* 2023, **382**, 284-289.
17. S. M. Park, M. Wei, J. Wu, H. R. Atapattu, F. T. Eickemeyer, K. Darabi, L. Grater, Y. Yang, C. Liu, S. Teale, B. Chen, H. Chen, T. Wang, L. Zeng, A. Maxwell, Z. Wang, K. R. Rao, Z. Cai, S. M. Zakeeruddin, J. T. Pham, C. M. Risko, A. Amassian, M. G. Kanatzidis, K. R. Graham, M. Gratzel and E. H. Sargent, *Science* 2023, **381**, 209-215.

18. H. Li, C. Zhang, C. Gong, D. Zhang, H. Zhang, Q. Zhuang, X. Yu, S. Gong, X. Chen, J. Yang, X. Li, R. Li, J. Li, J. Zhou, H. Yang, Q. Lin, J. Chu, M. Gratzel, J. Chen and Z. Zang, *Nat. Mater.* 2023, **8**, 946-955.
19. X. Zheng, Z. Li, Y. Zhang, M. Chen, T. Liu, C. Xiao, D. Gao, J. B. Patel, D. Kuciauskas, A. Magomedov, R. A. Scheidt, X. Wang, S. P. Harvey, Z. Dai, C. Zhang, D. Morales, H. Pruett, B. M. Wieliczka, A. R. Kirmani, N. P. Padture, K. R. Graham, Y. Yan, M. K. Nazeeruddin, M. D. McGehee, Z. Zhu and J. M. Luther, *Nat. Energy* 2023, **8**, 462-472.
20. R. Chen, J. Wang, Z. Liu, F. Ren, S. Liu, J. Zhou, H. Wang, X. Meng, Z. Zhang, X. Guan, W. Liang, P. A. Troshin, Y. Qi, L. Han and W. Chen, *Nat Energy* 2023, **8**, 839–849.
21. Q. Cao, T. Wang, X. Pu, X. He, M. Xiao, H. Chen, L. Zhuang, Q. Wei, H. L. Loi, P. Guo, B. Kang, G. Feng, J. Zhuang, X. Li and F. Yan, *Adv. Mater.* 2024, 2311970.
22. Z. Jiang, D. Wang, J. Sun, B. Hu, L. Zhang, X. Zhou, J. Wu, H. Hu, J. Zhang, W. C. H. Choy and B. Xu, *Small Methods,* **8**, 2300241.